Draft version August 26, 2004
Preprint typeset using LaTeX style emulateapj

AN IONIC ABSORBER AND NON-RELATIVISTIC REFLECTOR IN THE SEYFERT 1 GALAXY MCG -6-30-15

A. Kinkhabwala[1], S.M. Kahn[1], J.R. Peterson[1], M.F. Gu[2,3]

Draft version August 26, 2004

ABSTRACT

We perform a variability analysis of the complex X-ray spectrum (0.3 – 12 keV) of the Seyfert 1 galaxy MCG -6-30-15 using recent observations with *XMM-Newton* PN and RGS. Its variable spectrum is remarkably consistent at high spectral resolution with a simple model of a component with varying normalization (but no change in spectral shape) plus a constant component. The variable component is well fit by a power-law with (non-variable) ionic absorption from ions spanning a large range in ionization. The constant component exhibits a hard power-law-like component with near-neutral Fe Kα emission line and near-neutral Fe K edge (both consistent with reflection by distant Compton-thick material) plus a softer, emission-line-rich component (explained, at least in part, as line reemission from the ionic absorber). Notably, our model for MCG -6-30-15 *does not* require the following: (1) a soft excess due to a disk blackbody or relativistically-broadened C, N, or O Lyα lines, (2) a relativistically-broadened Fe Kα line, or (3) dust absorption. Ionic absorption in MCG -6-30-15 is similar to ionic absorption in the Seyfert 1 galaxy NGC 3783. Also, the observed constant line reemission is consistent with the inferred level of absorption. The constant component overall is somewhat reminiscent of the spectra of typical Seyfert 2 galaxies, such as NGC 1068, for which line reemission in the ionic absorber plus a hard reflection component (including Fe Kα and an Fe K edge) are also observed, providing tentative evidence for a particularly simple X-ray version of the unified model of active galactic nuclei.

Subject headings: galaxies: active — galaxies: individual (MCG -6-30-15, NGC 3783, NGC 1068), galaxies: Seyfert — techniques: spectroscopic — X-rays: galaxies

1. INTRODUCTION

MCG -6-30-15 is a Seyfert 1 galaxy that exhibits a particularly complex, highly-variable X-ray spectrum.

In the hard X-ray regime around 6 keV, an *ASCA* observation of MCG -6-30-15 revealed an Fe Kα emission line with apparently complex structure, which was interpreted by Tanaka et al. (1995) as a relativistically-broadened, fluorescent Fe Kα line from the inner regions of the accretion disk. This result, in particular its strong clean signature with a hint of underlying structure (the "red horn"), motivated further studies of this source. A few years later, Guainazzi et al. (1999) resolved the Fe K-shell dip due to the Compton-thick reflector and also claimed detection of a similar broadened Fe Kα feature in a *BeppoSAX* observation. Recent spectra of MCG -6-30-15 obtained by *XMM-Newton* and *Chandra* have produced a flurry of papers, several of which, for the Fe Kα region, also claim detection of a relativistically-broadened Fe Kα line (e.g., Wilms et al. 2001, Lee et al. 2002, Fabian et al. 2002; Fabian & Vaughan 2003). In these high-resolution studies, the shape of the broadened line is consistent with a smooth, featureless red wing (i.e., no "red horn").

In the soft X-ray regime, Branduardi-Raymont et al. (2001) proposed that the complex features observed in the *XMM-Newton* RGS spectra could similarly be explained as relativistically-broadened Lyα emission lines of O, N, and C. Lee et al. (2001) disputed this interpretation for the particular case of the relativistic O Lyα line, arguing that the sharp drop at 17.8 Å was more likely due to neutral Fe locked in dust grains as well as the photoelectric edge and near-edge resonance lines from He-like O from the warm absorber (hence, the "dusty warm absorber"). Lee et al. (2001) also required a soft excess explainable as a modified blackbody. Sako et al. (2003) countered, arguing primarily that the putative Fe dust grains, if at all similar to dust grains observed in our own Galaxy, should also produce a large neutral O K-shell edge at 23.5 Å (features such as a Si K-edge from silicate dust grains should also be present). Therefore, if dust is responsible for the observed opacity, it must be rather peculiar dust composed primarily of Fe.

High-resolution X-ray spectra of some other Seyfert 1 galaxies, which show discrete absorption features roughly comparable to MCG -6-30-15, appear less ambiguous. Their X-ray spectra can be fit with a model requiring

[1]Columbia Astrophysics Laboratory, Columbia University, 550 West 120th Street, New York, NY 10027; ali@astro.columbia.edu, skahn@astro.columbia.edu, jrpeters@astro.columbia.edu
[2]Center for Space Research, Massachusetts Institute of Technology, Cambridge, MA 02139; mfgu@space.mit.edu
[3]Chandra Fellow

only ionic absorption of an intrinsic power-law spectrum (e.g., NGC 3783, Blustin et al. 2002, also see below; and NGC 7469, Blustin et al. 2003). This suggests that the intrinsic spectra (before passing through the absorber) of at least certain Seyfert 1 galaxies are similar to the featureless power-law spectra observed from many quasars.

In fact, recent, CCD-resolution variability studies with *ASCA* and *XMM-Newton* PN of the X-ray spectrum of MCG -6-30-15 appear consistent with this simple absorbed power-law picture as well. These studies find that a varying absorbed power-law component plus a nonvarying harder component (Shih et al. 2002; Fabian & Vaughn 2003) is consistent with the data. In particular, by calculating the difference spectrum between high- and low-state spectra, Fabian & Vaughan (2003) found that the spectrum from 3–10 keV is consistent with a simple (unabsorbed) power-law. Importantly, this power-law continuum, when extrapolated to lower energies (and with Milky Way absorption taken into account), remained well above the data at all points, suggesting that the shape of the variable component might indeed be explained solely by absorption. Attenuation by an absorber is therefore more important than emission from any additional soft-excess component.

We pursue a similar variability analysis of the *XMM-Newton* PN spectra, but this time we also include the corresponding high-resolution RGS spectra. We verify, at high-resolution, that the variable spectrum of MCG -6-30-15 can be explained by a component with variable normalization (but no change in spectral shape) and a constant component. The variable component can be well fit with ionic absorption (spanning a wide range in ionization) of a simple power law; the level of ionic absorption is similar to that observed in the Seyfert 1 galaxy NGC 3783. The constant component exhibits a hard power-law-like spectrum with near-neutral Fe Kα emission line and near-neutral Fe K edge (consistent with reflection by a distant Compton-thick medium), along with a softer, emission-line-rich component (explained, at least in part, by reemission in the ionic absorber). It is, overall, reminiscent of non-variable Seyfert 2 spectra, such as NGC 1068 (Kinkhabwala et al. 2002), suggesting a particularly simple X-ray version of the unified model of AGN.

The outline of this paper is as follows. In §2, we describe the observations and spectral extraction. In §3, we emphasize the importance of absorption from ions spanning a wide range of ionization for the X-ray spectrum of MCG -6-30-15, using the X-ray spectra of the Seyfert 1 galaxy NGC 3783 for comparison. In §4, we present our spectroscopic variability analysis, discussing, in turn, the variable component and the constant component. A comparison of the constant component with the X-ray spectrum of the prototypical Seyfert 2 galaxy NGC 1068 is also performed. Finally, in §5, we discuss the implications of our results.

2. OBSERVATIONS AND SPECTRA

MCG -6-30-15 has been observed by both *Chandra* and *XMM-Newton*, with all observations to date now publicly available. We concentrate in particular on the RGS and PN spectra from *XMM-Newton* revolutions 301, 302, and 303 (over the period 2001 July 31 – 2001 August 5), which have a total exposure of 336 ks. Using 100 s bins, we have selected low-background good-time-intervals (GTIs) jointly using the RGS and PN light curves (PN observations use small window mode). The final GTI light curve for the PN is shown in Fig. 1.

MCG -6-30-15 is clearly highly variable, spanning a roughly factor-of-four range in flux during these observations. The solid line in Fig 1 subdivides the observations into low and high states, with the position of the line chosen to correspond to equal total PN counts for the low state as for the high state. The average fluxes in the low and high states are shown as the upper and lower dashed lines. Using standard *XMM-Newton* Science Analysis System v5.3 (SAS) routines, RGS and PN spectra have been extracted with all of the GTI, the high-state GTI, the low-state GTI, and, finally, the very-low-state GTI (with PN count rates less than 12 counts s^{-1}).

We also discuss *Chandra* HETGS observations of both MCG -6-30-15 (total exposure 125 ks; ObsID 433) and NGC 3783 (total exposure 889 ks; ObsID 373, 2090, 2091, 2092, 2093, and 2094). We discuss only the combined $m = \pm 1$ MEG spectra (extracted using CIAO v2.3). The *XMM-Newton* RGS and PN spectra of the prototypical Seyfert 2 galaxy NGC 1068 (Kinkhabwala et al. 2002) are also shown and discussed.

All plotted spectra have already been shifted to the source frame using their respective cosmological redshifts of $z = 0.00775 \pm 0.00005$ for MCG -6-30-15 (Fisher et al. 1995), $z = 0.00973 \pm 0.00001$ for NGC 3783 (Theureau et al. 1998), and $z = 0.00379 \pm 0.00001$ for NGC 1068 (Huchra, Vogeley, & Geller 1999). Where applicable, local Milky Way opacities of N_H =4.1e20 (MCG -6-30-15), 8.5e20 (NGC 3783), and 3.5e20 (NGC 1068) have been assumed (Dickey & Lockman 1990).

3. IONIC ABSORPTION

We focus in this section on a comparison between MCG -6-30-15 and the similar Seyfert 1 galaxy, NGC 3783. We argue the importance of absorption features due to ions spanning a wide range in ionization in both spectra.

3.1. *Silicon*

In Fig. 2, we show the 6–8 Å region of the *Chandra* MEG spectra (combined $m = \pm 1$ orders) of MCG -6-30-15 and NGC 3783. This region contains the important 1s→2p K-shell line absorption series of Si (e.g., Behar & Netzer 2002). For NGC 3783, there is clear detection of all relevant charge states of Si, from one to nine electrons (Kaspi et al. 2002). In MCG -6-30-15, we note that, despite the overall worse signal-to-noise, Si charge states from one to six or seven electrons are also detected.

Using XSTAR (Kallman & Bautista 2001; Bautista & Kallman 2001), we have calculated the fractional ionic abundances of all important ions, assuming an optically-thin medium irradiated by a power-law photon luminosity spectrum $L_\gamma(E) = AE^{-2}$ (e.g., in units photons s^{-1} keV^{-1}). The relative fractional ionic abundances of the different elements (the only quantities we will be concerned with) are largely independent of the details of the irradiating flux spectrum. In Fig. 3, we show the fractional ionic abundances versus log ionization parameter ($\xi = L/nr^2$, where L is the bolometric luminosity above 13.6 eV, n is the number density, and r is the radius from the source), with higher ionization parameter corresponding to higher ionization. At very high ξ, all ions are completely stripped of their electrons, whereas at very low ξ, all ions asymptote to their neutral charge states. The range in Si from one to nine electrons implies a range in ionization parameter of $\log\xi \sim 0$–3. Ions of other elements which have significant fractional abundances in this ionization range should also naturally be present and contribute to absorption.

3.2. *Iron Opacity*

Due to a convenient numerical coincidence, the measured column densities in Si correspond very closely to the column densities expected from Fe ions in the same ionization range. As noted above, the observed ionization range represented by Si ions with 1 to 9 electrons is $\log\xi \sim 0$–3, which corresponds to Fe ions with 2 to 20 electrons. Si, therefore, acts as a clean tracer (due to the absence of any other significant features in this spectral region) of the contribution of Fe ions to the opacity. Due to the insufficient signal-to-noise in MCG -6-30-15, not to mention its multiple velocity components (see Fig. 2) and its possible contribution from line reemission (see below), robust column densities for the Si ions are hard to obtain. However, the presence of a range in Si in this source is indisputable, and column densities on the order of 10^{16} cm^{-2} are roughly compatible with both spectra (as we demonstrate below for NGC 3783 in Figs. 6 and 7).

We show the opacity due to the full range of Fe ion species (from 1 to 26 electrons) with each ionic column density equal to 1e16 (4e16 cm^{-2}) in the top (bottom) panels of Fig. 4. A velocity width of $\sigma_v = 100$ km s^{-1} is also assumed. For 1e16 cm^{-2}, Fe opacity leads to a ~10% drop at ~ 17.5 Å (due to the near-neutral species), with myriad absorption features shortward of this drop. A gentle rise back to unity at around 2 Å (~ 6 keV) comes from the accumulated L-shell photoelectric edges with opacity at short wavelengths due mostly to higher-ionization species (L-shell Fe ions). On the other hand, for 4e16 cm^{-2}, the drop at 17.5 Å of 50% is far more precipitous with significant opacity all the way to 2 Å (6 keV).

3.3. *Full Spectra of MCG -6-30-15 and NGC 3783*

The full MEG (combined $m = \pm1$ order) spectra (1–30 Å) of both MCG -6-30-15 and NGC 3783 are shown in Fig. 5. These spectra reveal a forest of absorption lines due to multiple charge states of all the elements (especially Fe), as is expected from the observed range in Si (see Kaspi et al. 2002 for detailed line IDs for NGC 3783). Many of the same absorption features are observed in both spectra (note that due to differing and multiple blueshifts of the absorbers in these two galaxies, lines are *not* expected to line up exactly). Of particular interest are the different shapes of these two spectra in the region around 17.5 Å, which corresponds to the onset of the Fe L-shell transitions; in MCG -6-30-15, a far more precipitous drop is observed at slightly longer wavelength than for NGC 3783. This could be due to significant column densities of near-neutral Fe, a large He-like O column density, or some combination.

3.4. *NGC 3783 Fit Using Ionic Absorption of a Power Law*

Our fit to the MEG spectrum of NGC 3783 is given in Fig. 6, using only ionic absorption of a simple power law. Specifically, we employ the model XIABS (Kinkhabwala et al. 2003) in XSPEC (Arnaud 1996), which calculates column densities based on a user-defined distribution in ionization parameter. The fractional ionic abundances versus ionization parameter used by this model are those shown in Fig. 3. We assume a flat distribution in $\log\xi$ from 0.2 to 4.0, along with a total hydrogen column density of $N_H = 3e22$ cm^{-2} (including H I and H II); a power-law slope of $\Gamma = 1.8$ is also assumed. Abundances used for intrinsic absorption and for the local Milky Way absorption are those recommended by Wilms, Allen, & McCray (2000). The derived ionic column densities are shown in Fig. 7. It is surprising how well this extremely simple ionization distribution (with fixed abundances) reproduces the features of the spectrum. See Blustin et al. (2002) for a similar fit to the *XMM-Newton* RGS and PN spectra of NGC 3783, again using only ionic absorption of a power law.

The total opacity due to the postulated ionic absorber is shown in Fig. 8. Absorption is significant in all spectral regimes. In Fig. 9, a zoomed-in view of the Fe K region reveals multiple absorption lines created by the entire series of Fe ions employed to fit the line-rich L-shell region (roughly between 9 and 18 Å). These transitions are difficult to detect with *Chandra* or *XMM-Newton*. They may be created in the absorber or in the reflecting medium (the likely origin of the bright Fe Kα emission line). In fact, a strong dip in the data is observed blueward of the Fe Kα line, which is significantly deeper than the ionic Fe column densities we have employed for the absorber. From performing fits using ionization distributions weighted towards higher ionization states, which increases basically only the Fe L-shell column densities and K-shells of mid-Z ions such as Si and S, the depth of this feature can be completely accounted for. The data appear to require more K-shell Si anyway (see Fig. 6). Such a distribution, weighted towards higher ionization parameter, was employed by Blustin et al. (2002) to fit the *XMM-Newton* PN and RGS spectra.

We note that the level of the power law may be contaminated by the presence of an additional hard reflection component. A similar variability analysis as is undertaken below for MCG -6-30-15 may reveal the level of the reflection component in NGC 3783, though the effects of this component appear less severe in NGC 3783 due primarily to the harder intrinsic power law in this source ($\Gamma = 1.8$ for NGC 3783 versus $\Gamma = 2.3$ for MCG -6-30-15, see §4.1).

4. SPECTROSCOPIC VARIABILITY ANALYSIS

In this section, we describe the results of our time-resolved spectral analysis of MCG -6-30-15. Shown in Fig. 10 are the full spectra, high-state spectra, low-state spectra, and very-low-state spectra from the PN and combined RGS1 and RGS2 (spectral extraction described in §2). Note, in particular, the hardening of the spectrum and increased significance of the Fe Kα line (6.4 keV) and Fe K edge (7.0 keV) as the flux level decreases. Also note the change in equivalent width of the O VIII Lyα line at 19 Å, which is clearly observed as a deep absorption feature in the high state, but in the very-low-state is seen in emission. This is discussed at much greater length below.

As mentioned above, it has been suggested that the complex variability in the spectrum of MCG -6-30-15 can be fit with a simple model of a component with variable normalization (but no change in spectral shape) plus a constant component (Shih et al. 2002; Fabian & Vaughan 2003). In order to probe this assertion we have calculated the difference spectrum from the high-state and low-state spectra. The counts in both spectra (at least for the PN spectra) have been equalized to optimize the uncertainty, as described in §2. Further optimization is possible (e.g., exclusion of intervals lying close to the solid line), but it seems unlikely to improve the spectral uncertainty significantly.

The difference spectra from subtracting the low-state from the high-state are shown in Fig. 11. Difference spectra constructed by subtracting the very-low-state spectra from the high-state spectra are also shown, scaled by 0.55. Note the concordance of the two spectra, particularly in regions showing large line absorption (the most visible being O VIII at 19 Å). This proves, at high resolution, that (1) the variable spectrum does not change shape as it varies, and (2) any additional component must be remarkably constant, both confirming the simple variability model postulated above. This result serves as the basis of this paper, allowing us to define and probe the variable and constant components as described below.

4.1. *Variable Component*

A power law fitted to the high-energy end (above 4 keV) with index $\Gamma = 2.3$ is shown on top of the difference spectra (high-state minus low-state) in Fig. 12. A zoomed-in view of the Fe K region is given in Fig. 13, showing the absence of any emission or absorption features above 4 keV (Fabian & Vaughan 2003). The fit shown in red is described below.

The total ionic plus Milky Way opacity is given in Fig. 14. A zoomed-in view of the hard region, showing the absence of discrete absorption features above 4 keV is shown in Fig. 15.

A zoomed-in view of the 15–25 Å region of the RGS spectrum is provided in Fig. 16. We point out the importance of discrete O K-shell 1s$\rightarrow$2p absorption features. The number of transitions plus the fact that MCG -6-30-15 is known to have two velocity components (one at near systemic and the other at -1900 km s^{-1}), suggest that line blanketing may be important in this region.

Our fit to the difference spectra using only ionic absorption of the $\Gamma = 2.3$ power law is also shown in Fig. 12 (in red). Ionic column densities for this fit were chosen "by eye." The fit itself is meant only to be suggestive. We show the column densities we use in Fig. 17. We note that the high ionic opacity considered here makes the fitting procedure very sensitive to relatively small changes in the many parameters we are using (in particular, the large amount of near-neutral Fe can easily be traded off with more H- and He-like O). However, we argue that at least the bulk of the spectrum can be accounted for in a reasonable absorption model. Robust characterization of the residuals is of great interest; understanding the origin of the ionization distribution would in particular simplify the fitting procedure considerably. But these goals must be left for future, more detailed studies.

4.2. *Constant Component*

We would now like to determine the shape of the constant component. We might simply assume that the very-low-state is representative of the constant component, but even in this state, it is impossible to rule out a contribution from the variable component. (If in the very-low-state, the variable component *were* completely absent, one might expect the source to occasionally idle — i.e., remain in this state for some reasonable amount of time, producing an observable flux floor — rather than dip as observed in Fig. 1.)

However, despite this uncertainty, a robust upper limit to the constant component flux and shape is given by the very-low-state spectra and a corresponding robust lower limit is obtained by scaling the difference spectra (representing the shape of the variable component) to be coincident with, but nowhere higher than, the full spectra (as shown in Fig. 18), and then subtracting. These limits are shown in Fig. 19.

We particularly make note of some interesting discrepancies labelled in the bottom panels of Figs. 18 and 19. If the constant component is assumed to lie behind the ionic absorber and to have a fairly continuous shape, then the discrete absorption features observed for both the variable component and for the constant component should have equal equivalent width, implying the same equivalent width for the full spectra as well. However, this is not the case. Note, in particular the discrete absorption of O VIII Lyα, which is very deep in the difference spectra, but a factor of a few shallower in the full spectra. The same case can be made for the other labelled features corresponding to O VII RRC/Fe XVII, O VII rif, and C Lyα (for the labelled N lines, the case is not as strong). Upon subtraction, these features will arise as high-equivalent-width lines, as clearly seen (despite overall spectral uncertainty) in Fig. 19.

Also, in both limiting spectra, a rather flat power-law like spectrum with neutral Fe Kα line at 6.4 keV and Fe K edge around 7.0 keV is observed. These features appear consistent with a spectrum produced by reflection of the power law in near-neutral Compton-thick material, as will be elaborated upon below.

As a final maneuver, we divide out the total absorption (due to both absorption in the ionic absorber at the source and Milky way opacity) using the difference spectra itself and the $\Gamma = 2.3$ power law given in Fig. 13 (we assume opacity above 4.0 keV is negligible in order to avoid any artifacts of this process at those energies). The spectra obtained are shown in Fig. 20. Dividing out the total opacity is not strictly valid because of possible line saturation and the likely origin of some fraction of the constant component (in particular the line emission) in the ionic absorber itself. Estimation of the latter effect is described in Kinkhabwala et al. (2003).

In the top panel of Fig. 20, we show a simple model of reflection from Compton thick material; a zoomed-in view with error bars is shown in Fig. 21. We also give the average $\Gamma = 2.3$ power law estimated from the full spectrum. The reflection component is calculated assuming the average power law reflects off an infinite, cold (neutral), face-on reflector (XSPEC model PEXRAV), with 350% reflectivity. The additional reflectivity (over 100%) is most easily explained by source variability, i.e., the source may simply have been a factor of a few brighter in the past (though, for other possibilities, see Fabian & Vaughan 2003). The reflection model is provided only for illustrative purposes. Consideration of a more ionized reflector (e.g., Ballantyne, Vaughan, & Fabian 2003) would remove some of the Fe L-shell opacity (in much the same way as shown in Fig. 4), and would thereby steepen and increase the flux in the reflection spectra above 0.7 keV. The jagged features in the PN spectra from 1.8 to 3 keV, as noted in §2, are most likely due to miscalibrated Au M-shell and/or Si K-shell, but could be partially associated with discrete absorption in the reflector or to reemission in the reflector or ionic absorber. The Fe Kα line most likely originates in the reflecting medium (though some fraction of the line might also arise in the ionic absorber).

The Fe K region of the estimated constant component is compared with the Fe K region of the prototypical, non-variable Seyfert 2 galaxy, NGC 1068, in Fig. 22. The Fe Kα complex in NGC 1068 includes a near-neutral Fe Kα and H- and He-like Fe 2p$\rightarrow$1s lines, as clearly resolved in high-resolution spectra taken with *Chandra* (Brinkman et al. 2002; Ogle et al. 2003) and partially resolved in the PN spectrum shown here. The neutral Fe Kα line has a much larger equivalent width in the spectrum of NGC 1068 than in the constant spectrum of MCG -6-30-15; the Fe K edge is also not as pronounced (though a deficit of counts above $\sim$8.0 keV is present). Fabian & Vaughan (2003) fit a relativistically blurred ionized disk model to the very-low-state spectrum (approximately the green curve in Fig. 21). The lower limit to the constant spectrum, however, appears to have no significant asymmetry to the Fe K line and could be consistent with a non-relativistic reflector. The green curve may still be significantly contaminated by the variable power-law component which could easily mimic a broad red wing to the relativistic line. On the other hand, a slightly variable red wing to the Fe K (less variable than the power-law component) could be present (as advocated in Fabian & Vaughan 2003). Distiguishing between the two possibilities is challenging, but arguably there is no clear spectroscopic signature that necessarily points towards the existence of a relativistic reflector.

In the unified model of AGN, for which NGC 1068 provided the first and most significant example, the view to the nucleus for Seyfert 2 galaxies is highly obscured. For NGC 1068, the view is likely completely obscured. The hard power law observed from NGC 1068 is inconsistent with absorption of an intrinsic power law. This, coupled with the lack of variability, suggest an origin in reflection off of distant near-neutral Compton thick material. In the unified model, this hard region is naturally expected to be viewed in the Seyfert 1 direction. The shape of this spectrum in NGC 1068 corresponds fairly well with the upper and lower limits of the MCG -6-30-15 constant component.

Finally, in Fig. 23, line-rich spectra and models associated with reemission in the ionic absorber are shown. In the top panel, the PN and RGS spectra (with separation at 9 Å) are shown for NGC 1068 (Kinkhabwala et al. 2002). Such a spectrum is expected at some level from the absorbers in MCG -6-30-15 and NGC 3783. In the middle panel, we show the lower limit to the constant component in MCG -6-30-15, with the reemission due to the ionic absorber overplotted (assuming an isotropic cone with covering fraction $f = 0.1$; this component has also been multiplied by an additional factor of five). Finally, the reemission expected from the ionic absorber in NGC 3783 is shown in the bottom panel. The predicted reemission components in MCG -6-30-15 and NGC 3783 are clearly similar in nature to the soft regime of NGC 1068. Furthermore, line reemission is also a contributor to the constant spectrum in MCG -6-30-15. The additional factor of five required to fit the data may once again arise from the source having been brighter sometime in the recent past (as required above for the hard reflection component), al-though such a conclusion is somewhat dependent on the detailed geometry of the absorber.

5. DISCUSSION

Analysis of X-ray spectroscopic variability for MCG -6-30-15 has revealed that the simple model of a component with variable normalization (but constant spectral shape) plus a constant component is consistent at the highest spectral resolution. This has allowed us to probe in great detail the properties of the variable component, which we have shown to be consistent with a power law with ionic absorption, and the constant component, which is explainable, at least in part, as reflection in a Compton thick medium plus reemission in the ionic absorber. Comparison of the constant component with the prototypical Seyfert 2 galaxy, NGC 1068, provides tentative evidence for a particularly simple X-ray version of the unified model of AGN.

5.1. *Absence of a Soft Excess*

The fits employed above to describe the X-ray spectra of NGC 3783 and the variable component of MCG -6-30-15 only require ionic absorption of a power law, obviating the need for an additional soft excess (which had been postulated to arise from a modified blackbody or relativistically-broadened Lyα lines of O, N, and/or C). Given the likely contamination of high-energy X-ray spectra by a reflection component (as shown above for MCG -6-30-15) — which tends to flatten the inferred power law and thereby increases the significance of the putative soft excess — estimation of the true, intrinsic power law in other Seyfert 1 galaxies may also require a full spectroscopic variability analysis.

5.2. *Column Densities: Line Reemission and Unresolved Velocity Distributions*

As we have pointed out in the caption to Fig. 10, the equivalent widths of discrete absorption features (especially O VIII Lyα) decrease with decreasing flux. We have shown that this does not arise from variable absorption, but is instead consistent with constant line reemission from the ionic absorber. Column densities of individual ions based on their absorption line equivalent widths for the full spectrum are therefore likely to be severely contaminated by this line reemission, verifying the concerns of Lee et al. (2001). Complex line profiles (showing absorption and emission) from other Seyfert 1 galaxies verify the importance of reemission, as well as the importance of narrow velocity distributions unresolved at X-ray resolution, but clearly seen at UV resolution (e.g., Collinge et al. 2001). Estimation of column densities from discrete X-ray absorption is clearly highly uncertain. We note that line reemission may also provide a contaminant for observed UV absorption features from AGN. In particular, the well-known fact that UV lines are rarely observed to be "black" may simply reflect the additional contribution from constant line reemission in the absorber. This hypothesis can be simply tested in the manner described above for MCG -6-30-15 (creating and proving the constancy of shape of the difference spectrum and then subtracting the difference spectrum from the full spectrum).

5.3. *Detecting Dust*

Arguments against dust opacity in MCG -6-30-15 have already been reviewed in §1. On a more detailed level, we discuss the prospects of detection of the near-edge L-shell resonance structure arising from neutral Fe locked in solid dust grains. We note that the detailed near-edge resonance L-shell structure of near-neutral Fe ions is itself not completely known, though calculations are on-going. Therefore, robust discrimination of Fe ion near-edge resonance structure from resonance structure arising from neutral Fe locked in dust grains is at the very least extremely challenging (and, we believe, impossible for MCG -6-30-15, given its complicated absorption and strong evidence for near-neutral ions) even at the highest currently-available spectral resolution (*Chandra* HETGS). For these reasons, as well as those mentioned in §1, we favor an interpretation based solely on Fe ion opacity for MCG -6-30-15. However, we note that discrimination of these dust grain features in spectra with overall simpler (or better yet, completely absent) ionic absorption might still be possible.

5.4. *Variability Constraints*

Comparison of the difference spectra created by subtracting the low-state from the high-state and the very-low-state from the high-state shows that the variable spectrum retains its shape while varying. This puts a strong constraint on any variable absorption. Variability in individual lines is likely hard to detect given the broad ionization distribution required to explain the data. However, variability in the total continuum opacity especially at longer wavelengths, should be detectable for a *nearby* absorber such as an accretion disk atmosphere. This appears to be ruled out as well, favoring the scenario of absorption in a large-scale outflow, such as the outflow observed in NGC 1068 (Brinkman et al. 2002; Ogle et al. 2003), as well the extended outflows observed in other Seyfert 2 galaxies (Sako et al. 2000; Ogle et al. 2000; Sambruna et al. 2001).

5.5. *Reflection Component*

The region responsible for the hard regime (around Fe K) of the constant component likely lies at an equal or closer distance to the source as the absorbing medium (especially if this absorber is similar to the absorbers associated with the extended outflows observed from Seyfert 2 galaxies). In Seyfert 2 galaxies, representing the "side view," the continuum component plus Fe Kα line are unresolved, whereas the outflow is resolved at typically tens to hundreds of parsec (e.g., Brinkman et al. 2002, Ogle et al. 2003). Therefore, the hard regime of the constant component (associated with reflection in Compton-thick material) should experience the same absorption as the intrinsic continuum.

5.6. *Relativistically-broadened Emission lines*

We find that the data do not require the putative soft X-ray relativistic Lyα emission lines of C, N, and O. We have demonstrated that these features have a more likely origin as artifacts of absorption of the extrapolated variable power-law continuum observed above 4 keV. We have shown that a particular distribution of ionic column densities can reproduce these features. The importance of a range of Fe ions yields enough opacity to explain the sharp drop at 17.5 Å (Fe locked in dust grains is not required), though the opacity due to Fe can easily be traded off by adding more O K-shell opacity. A more detailed absorption fit to the variable component is left for the future.

We also find no clear evidence for a relativistically-broadened Fe Kα emission line in MCG -6-30-15. As we have shown, the combined effects of absorption and reflection can be complex and subtle. Ionic absorption possibly combined with a reflection spectrum (from distant material due to observed lack of variability) could easily mimic any smooth, relativitistically-broadened Fe Kα line. Even if relativistic lines are present in the spectra (and have the proper variability), in the absence of a discriminatory diagnostic, such as the elusive "red horn," distinguishing them from the above effects is, at best, very challenging.

We note that this discussion applies equally well to the case of Galactic black holes with putative relativistically-broadened Fe Kα lines, e.g., Cyg X-1 (Fabian et al. 1989; Miller et al. 2002a). In particular, we note that the high column densities (especially in Fe) inferred from the rich line absorption spectrum of Cygnus X-1 (e.g., Miller et al. 2002b) suggest that absorption may indeed by very important in this source.

5.7. *Ionization Distribution*

The rough correspondence of the predicted Seyfert-2-like spectra from the ionic column densities employed to fit NGC 3783 and MCG -6-30-15 once again illustrate the importance of a wide range in ionization generically present in AGN. For NGC 1068, spatially-resolved spectroscopy reveals that the observed distribution is due primarily to an orders-of-magnitude density distribution at each position in the absorbing medium (Brinkman et al. 2002; Ogle et al. 2003). The spatial coincidence of UV and optical emission in NGC 1068 also appears consistent with a continuous ionization distribution to even higher densities. The velocity coincidence of optical/UV absorbers with X-ray absorbers in the Seyfert 1 galaxies further argues for this interpretation as well. The origins of this density distribution are mysterious. Possibilities include a balancing of absorbing cloudlet creation/destruction or possible thermal instability effects. Though, reasonable magnetic field strengths tend to make a medium in photoionization equilibrium stable to isobaric perturbations (e.g., Bottorff et al. 1997; Bottorff, Korista, & Shlosman 2000). We suggest that magnetic fields might also be generically important for the creation and/or stabilization of the observed density distribution.

5.8. *Comparison MCG -6-30-15 and NGC 3783*

Though both NGC 3783 and MCG -6-30-15 exhibit a broad ionization distribution for their ionic absorbers, a detailed comparison reveals some noteworthy differences. In particular, the intrinsic power-law slope of 2.3 for MCG -6-30-15 is significantly steeper than the slope of 1.8 inferred for NGC 3783. Partly because of this, the hard reflection component in MCG -6-30-15 is more significant compared with its power-law component than is the case for NGC 3783. This difference in contrast likely underlies the fact that MCG -6-30-15 has been suggested to harbor a broadened Fe K line, whereas NGC 3783 is not thought to have such a feature. Also, the ionic absorber in NGC 3783 can be fit with a simple flat distribution in ionization, however, MCG -6-30-15 appears to require more either more near-neutral ions or more O absorption. More detailed investigation of these differences must be left for future studies.

5.9. *For the Future*

The spectroscopic variability analysis employed above — based on the first-order, testable hypothesis of a component with variable normalization (but no spectral change) plus a constant component, and consisting of the following steps: (1) construction of appropriate difference spectra, (2) verification of constancy of spectral shape of the variable component by comparing multiple difference spectra, and (3) estimation of the constant component — is of course broadly applicable for studies of any variable astrophysical source. In particular, further such studies with *XMM-Newton* and *Chandra* of both Seyfert 1 and Seyfert 2 galaxies are necessary to verify the simple unified model of AGN described above, which includes only ionic absorption of a variable, featureless, power-law continuum and a non-variable, hard reflection component (with associated fluorescent Fe Kα line and Fe K edge). Similar spectroscopic variability studies of the optical/UV spectra of AGN should also help disentangle the complex absorption/emission observed in this regime.

Finally, future observations with *Astro-E2* should provide an extremely interesting probe of the Fe K region. Through construction of the difference spectrum, *Astro-E2* should be able to reveal the discrete and continuous Fe K shell transitions expected from the inferred Fe L shell opacity required to fit the soft X-ray absorption in both NGC 3783 (Fig. 9) and MCG -6-30-15 (Fig. 15), in particular determining the relative importance of Fe L-shell opacity versus O K-shell opacity for the sharp drop in MCG -6-30-15 at 17.8 Å. Such a detection would help to further strengthen the model of absorption of a power-law versus the presence of a soft excess (from either a black-body or relativistically-broadened C, N, and O Lyα emission lines). It may also provide evidence for the range of near-neutral Fe species proposed above versus the existence of neutral Fe lock in dust grains. In addition, estimation of the constant component's Fe K shell region should also reveal the importance of complex absorption in the reflector versus the existence of a relativistically-broadened Fe Kα emission line. Though, given the ability of complex Fe K- and L-shell absorption in the reflector to mimic a smooth red wing, even with *Astro-E2*, the existence of a *constant* relativistically-broadened emission line may still be somewhat ambiguous.

We would like to thank M. Sako and A.C. Fabian for useful discussions. The Columbia University team is supported by NASA. AK acknowledges additional support from a NASA GSRP fellowship.

References

Arnaud, K.A. 1996, in ASP Conf. Ser. 101, Astronomical Data Analysis Software Systems V, ed. G.H. Jacoby & J. Barnes (San Francisco: ASP), 17

Ballantyne, D.R., Vaughan, S., & Fabian, A.C. 2003, MNRAS, 342, 239

Bautista, M., & Kallman, T.R. 2001, ApJS, 134, 139

Behar, E., & Netzer, H. 2002, ApJ, 570, 165

Blustin, A.J., Branduardi-Raymont, G., Behar, E., Kaastra, J.S., Kahn, S.M., Page, M.J., Sako, M., & Steenbrugge, K.C. 2002, 392, 453

Blustin, A.J. et al. 2003, A&A, 403, 481

Bottorff, M.C., Korista, K.T., & Shlosman, I. 2000, ApJ, 537, 134

Bottorff, M.C., Korista, K.T., Shlosman, I., & Blandford, R.D. 1997, ApJ, 479, 200

Branduardi-Raymont, Sako, M., Kahn, S.M., Brinkman, A.C., Kaastra, J.S., & Page, M.J. 2001, A&A, 365, 140

Brinkman, A.C., Kaastra, J.S., van der Meer, R.L.J., Kinkhabwala, A., Behar, E., Paerels, F.B.S., Kahn, S.M., Sako, M. 2002, A&A, 396, 761

Collinge, M.J. et al. 2001, ApJ, 557, 2

Dickey, J.M., & Lockman, F.J. 1990, ARA&A, 28, 215

Fabian, A.C., Rees, M.J., Stella, L., & White, N.E. 1989, MNRAS, 238, 729

Fabian, A.C. et al. 2002, MNRAS, 335, 1

Fabian, A.C., & Vaughan, S. 2003, accepted by MNRAS (astro-ph/0302288)

Fisher, K.B., Huchra, J.P., Strauss, M.A., Davis, M., Yahil, A., & Schlegel, D. 1995, ApJS, 100, 69

Guainazzi, M. et al. 1999, A&A, 341, L27

Huchra, J.P., Vogeley, M.S., & Geller, M.J. 1999, ApJS, 121, 287

Kallman, T.R., & Bautista, M. 2001, ApJS, 133, 211

Kaspi, S. et al. 2002, ApJ, 574, 643

Kinkhabwala, A., Sako, M., Behar, E., Kahn, S.M., Paerels, F.B.S., Brinkman, A.C., Kaastra, J.S., Gu, M.F., & Liedahl, D.A. 2002, ApJ, 575, 732

Kinkhabwala, A., Behar, E., Sako, M., Gu, M.F., Kahn, S.M., & Paerels, F.B.S. 2003, accepted by ApJ (astro-ph/0304332)

Lee, J.C., Iwasawa, K., Houck, J.C., Fabian, A.C., Marshall, H.L., & Canizares, C. 2002, ApJ, 570, 47

Lee, J.C., Ogle, P.M., Canizares, C.R., Marshall, H.L., Schulz, N.S., Morales, R., Fabian, A.C., & Iwasawa, K. 2001, ApJ, 554, 13

Miller, J.M, Fabian, A.C., Wojdowski, P.S., Reynolds, C.S., Ehle, M., Freyberg, M.J., van der Klis, M., Lewin, W.H.G., Sanchez-Fernandez, C., & Castro-Tirado, A.J. 2002, ApJ, 570, L69

Miller, J.M, Wojdowski, P.S., Schulz, N.S., Marshall, H.L., Fabian, A.C., Remillard, R.A., Wijnands, R., & Lewin, W.H.G. 2002, astro-ph/0208463

Ogle, P.M., Brookings, T., Canizares, C.R., Lee, J.C., & Marshall, H.L. 2003, A&A, 402, 849

Ogle, P.M., Marshall, H.L., Lee, J.C., & Canizares, C.R. 2000, ApJ, 545, L81

Sako, M., Kahn, S.M., Branduardi-Raymont, G., Kaastra, J.S., Brinkman, A.C., Page, M.J., Behar, E., Paerels, F., Kinkhabwala, A., Liedahl, D.A., & den Herder, J.W. 2003, accepted by ApJ (astro-ph/0112436)

Sako, M., Kahn, S.M., Paerels, F.B.S., & Liedahl, D.A. 2000, ApJ, 543, L115

Sambruna, R.M., Brandt, W.N., Chartas, G., Netzer, H., Kaspi, S., Garmire, G.P., Nousek, J.A., & Weaver, K.A. 2001, ApJ, 546, L9

Shih, D.C., Iwasawa, K., & Fabian, A.C. 2002, MNRAS, 333, 687

Tanaka, Y. et al. 1995, Nature, 375, 659

Theureau, G., Bottinelli, L., Coudreau-Durand, N., Gouguenheim, L., Hallet, N., Loulergue, M., Paturel, G., & Teerikorpi, P. 1998, A&AS, 130, 333

Wilms, J., Allen, A., & McCray, R. 2000, ApJ, 542, 914

Wilms, J., Reynolds, C.S., Begelman, M.C., Reeves, J., Molendi, S., Staubert, R., & Kendziorra, E. 2001, MNRAS, 328, L27

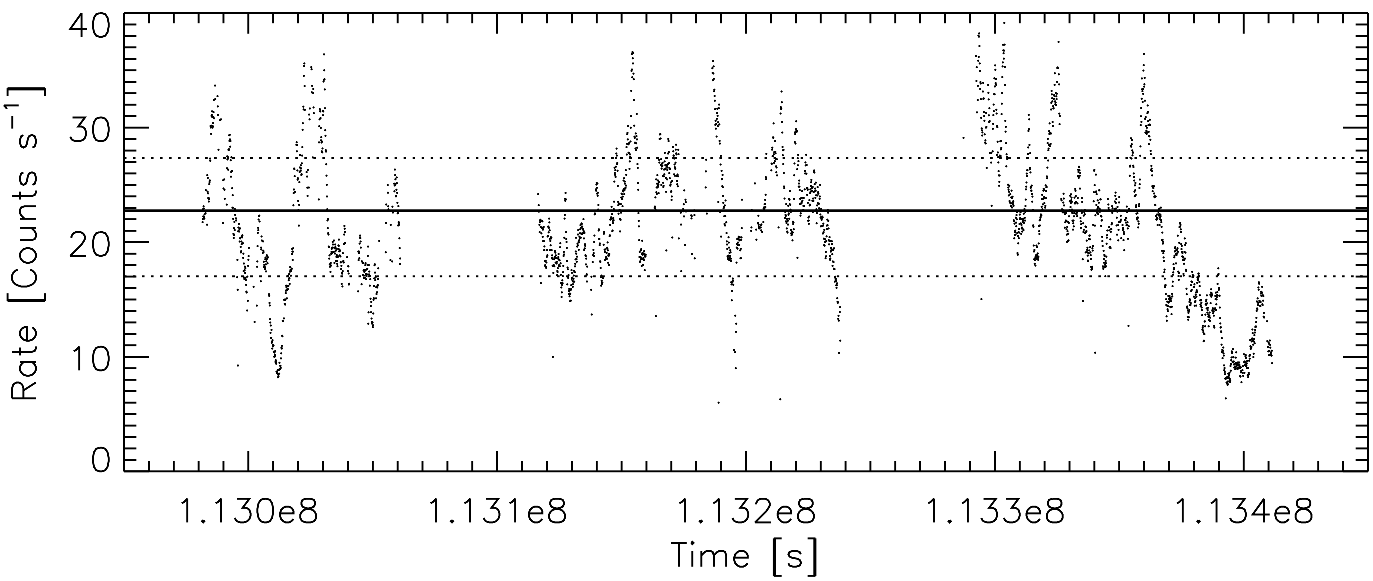

FIG. 1.— Total PN count rate for *XMM-Newton* observations of MCG -6-30-15 during revolutions 301, 302, and 303 using 100 s bins. The solid line denotes the division between the high and low state spectrum. Its position has been chosen to give the same total number of counts for both states. The dashed lines above and below the solid line respectively give the average rates for the high and low states. An additional very-low-state spectrum was calculated using only those intervals with rates less than 12 counts s^{-1}.

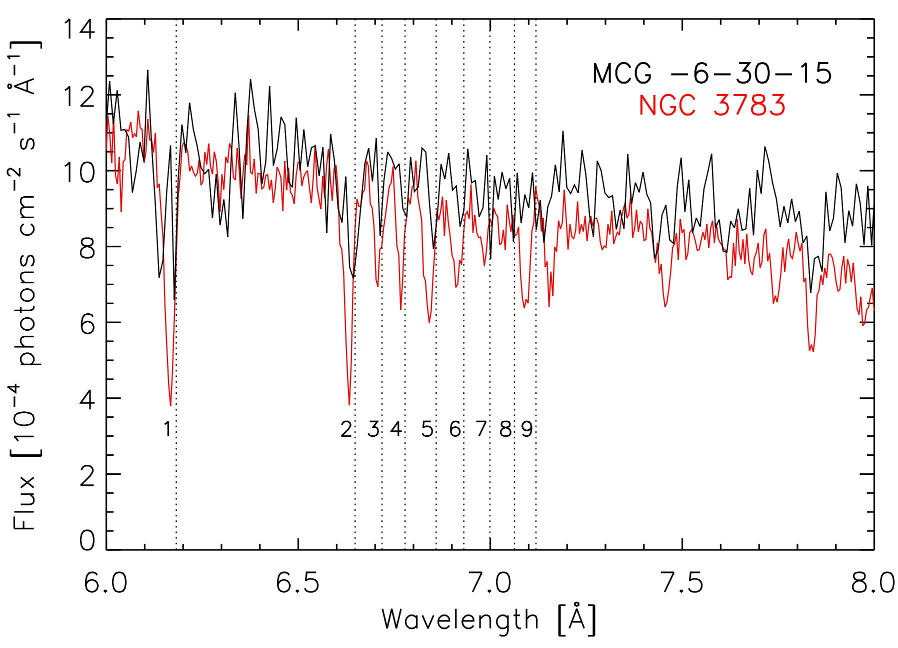

FIG. 2.— *Chandra* MEG source-frame spectra (combined $m = \pm 1$ orders) for both MCG -6-30-15 (black) and NGC 3783 (red) in the range of the K-shell Si line series, using 10 and 5 mÅ bins, respectively. Si charge states are labelled by the number of electrons (from 1 to 9). For NGC 3783, there appears to be only one velocity component (blueshifted by $\sim$700 km s^{-1}). All relevant Si charge states (1 to 9 electrons) appear. For MCG -6-30-15, two velocity components are present (see the H- and He-like lines), with one near the systemic velocity and the other blueshifted by roughly -1900 km s^{-1}. Si charge states with 1 to 6 or 7 electrons are present; noise prevents assessment of the presence of any further charge states.

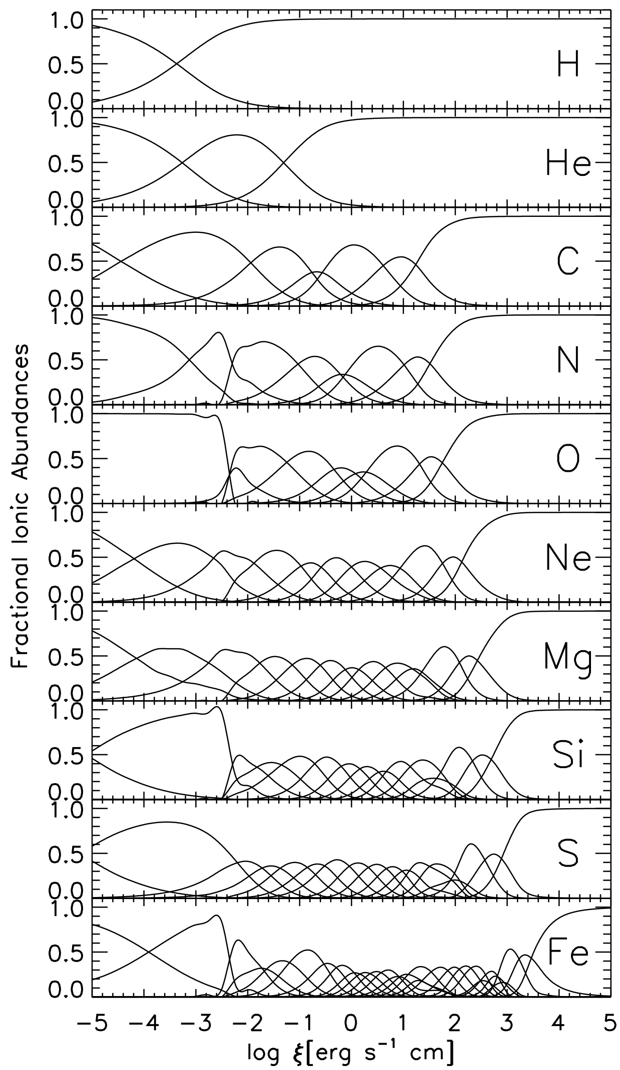

FIG. 3.— Fractional ionic abundance versus log ionization parameter, $\xi = L/nr^2$, calculated for optically-thin conditions in a medium irradiated by a $\Gamma = 2$ power law using XSTAR.

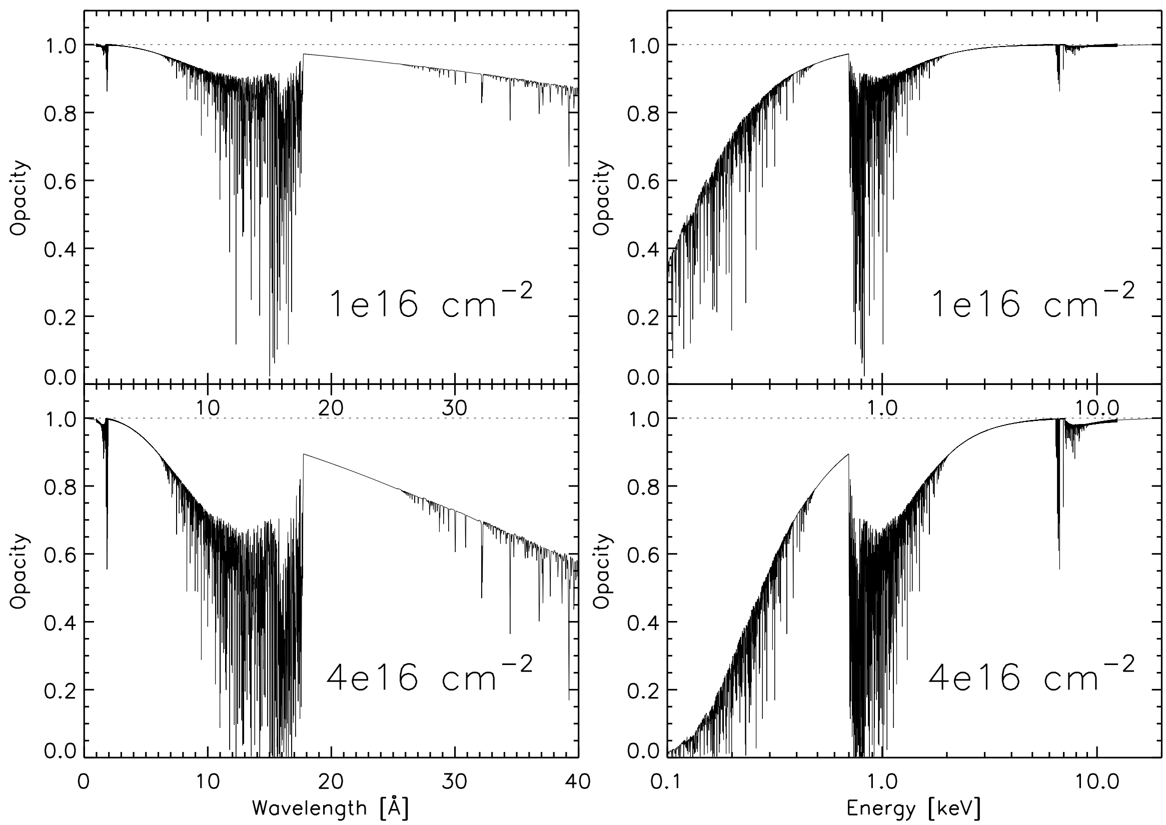

FIG. 4.— Opacity due to the full range of Fe ions (single electron to neutral), assuming each charge state has a column density of 1e16 cm^{-2} (top) and 4e16 cm^{-2} (bottom). A velocity width of $\sigma_v = 100$ km s^{-1} is assumed.

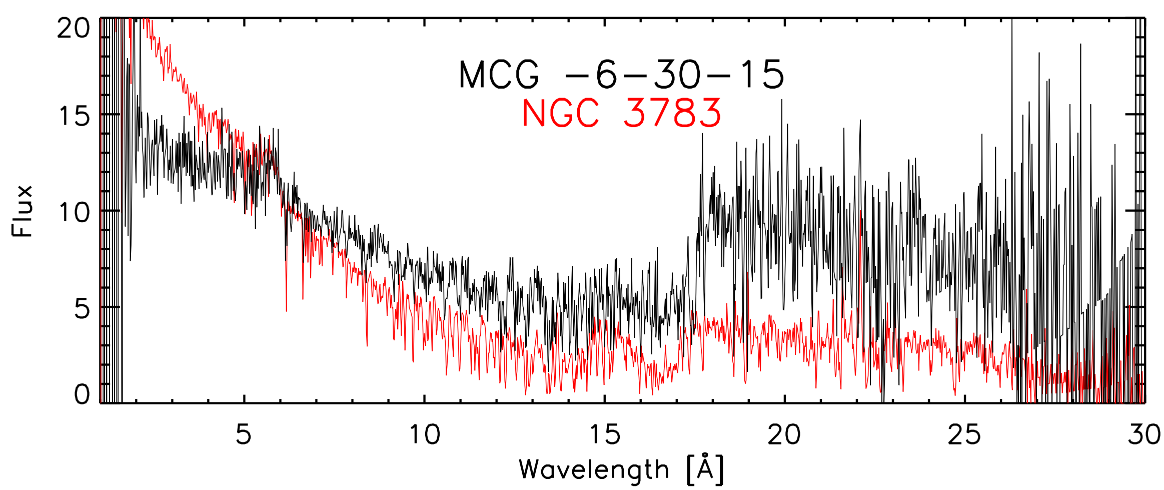

FIG. 5.— Same MEG spectra of MCG -6-30-15 and NGC 3783 as in Fig. 2, except shown over the full 1–30 Å MEG range and using 20 mÅ bins for both spectra. Note the prominent drop around 17.5 Å, which coincides with the beginning of the Fe L-shell. This drop is sharper and occurs at a slightly longer wavelength for MCG -6-30-15.

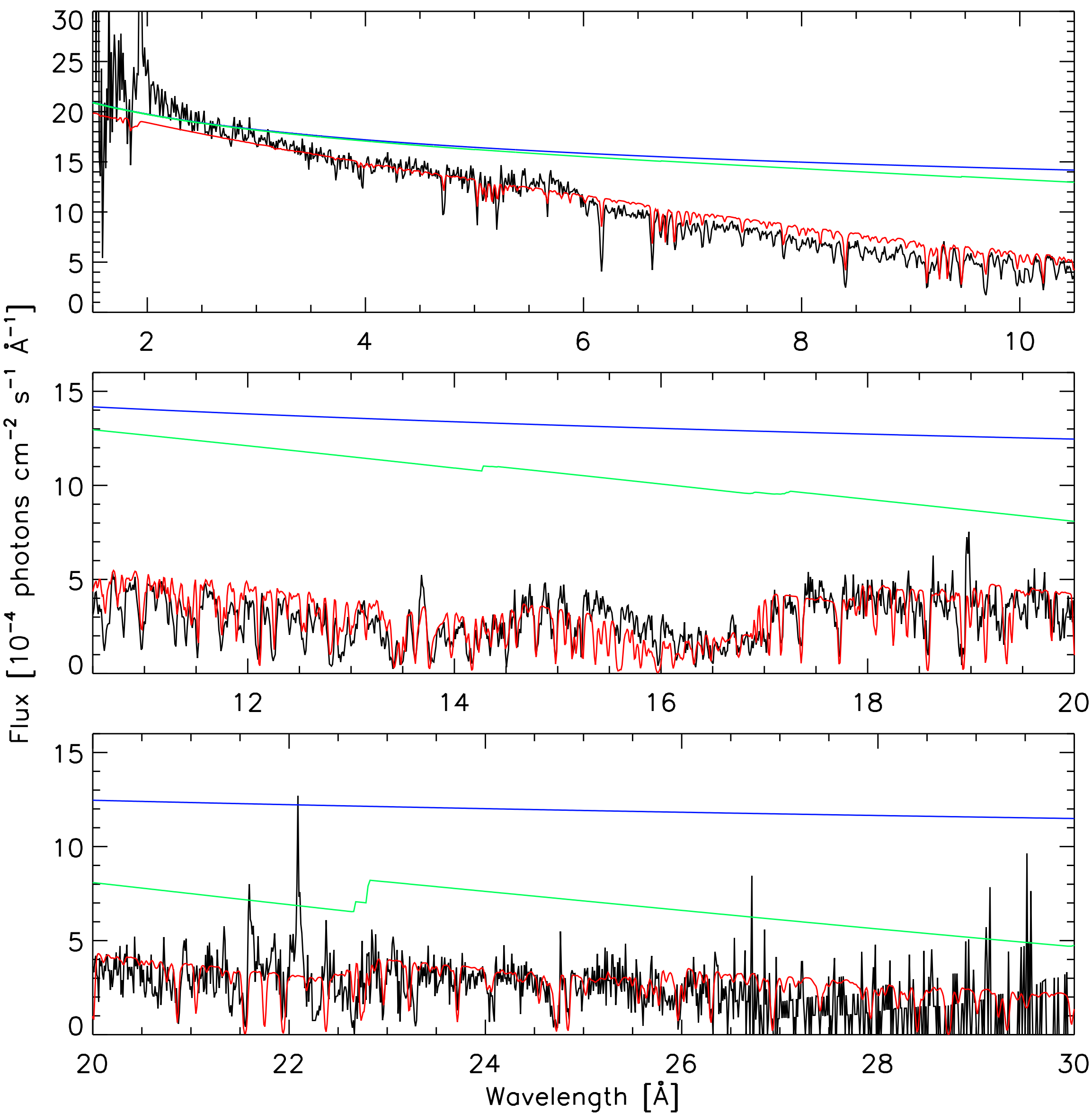

FIG. 6.— Source-frame MEG spectrum (combined $m = \pm 1$ orders) of NGC 3783 (black) using 5 mÅ bins. The intrinsic power law ($\Gamma = 1.8$) is shown in blue, the power-law with Milky-way absorption of $N_{\rm H} = 8.5\text{e}20$ cm^{-2} is shown in green, and the power-law with both Milky-way absorption and intrinsic ionic absorption is shown in red. For the ionic absorber, a velocity width of $\sigma_v = 100$ km s^{-1} has been assumed, as well as a blueshift of -700 km s^{-1}.

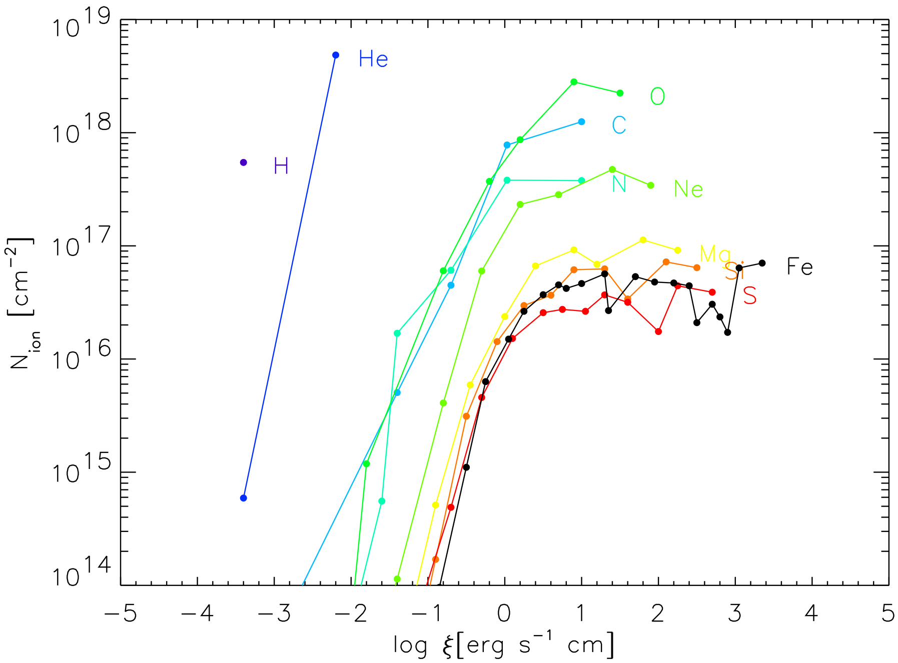

FIG. 7.— Ionic column densities versus log ionization parameter position of fractional ionic abundance peak (for neutral ions, we take the value of $\log \xi$ where fractional ionic abundance is a half) used to fit the spectrum of NGC 3783 (see Fig. 6).

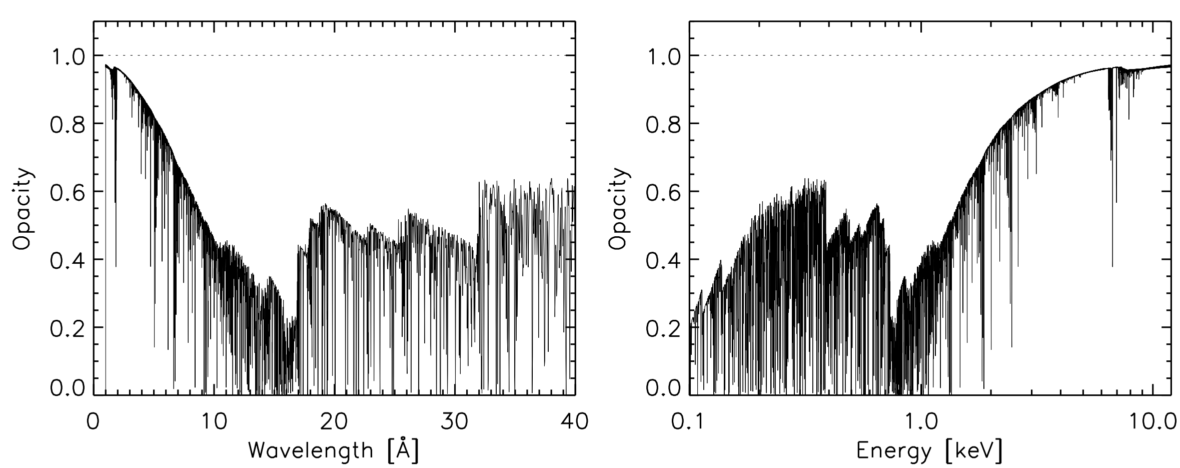

FIG. 8.— The opacity due solely to ionic absorption from the fit to NGC 3783 shown in Fig. 6. Additional opacity due to the Milky Way column density as well as the velocity blueshift have been removed.

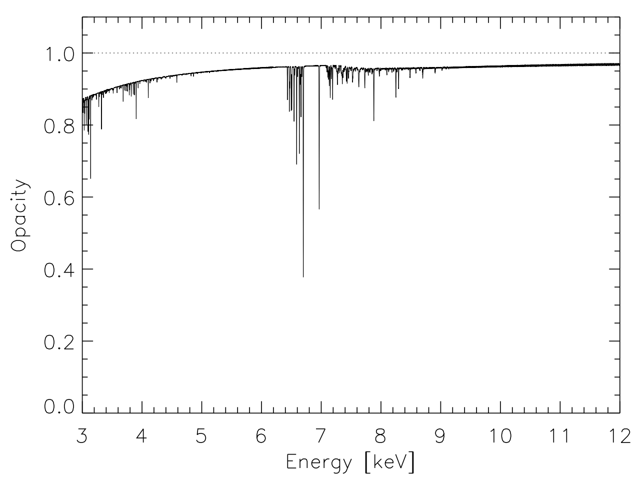

FIG. 9.— Predicted Fe K-shell opacity for NGC 3783 (zoomed-in view of right panel of Fig. 8).

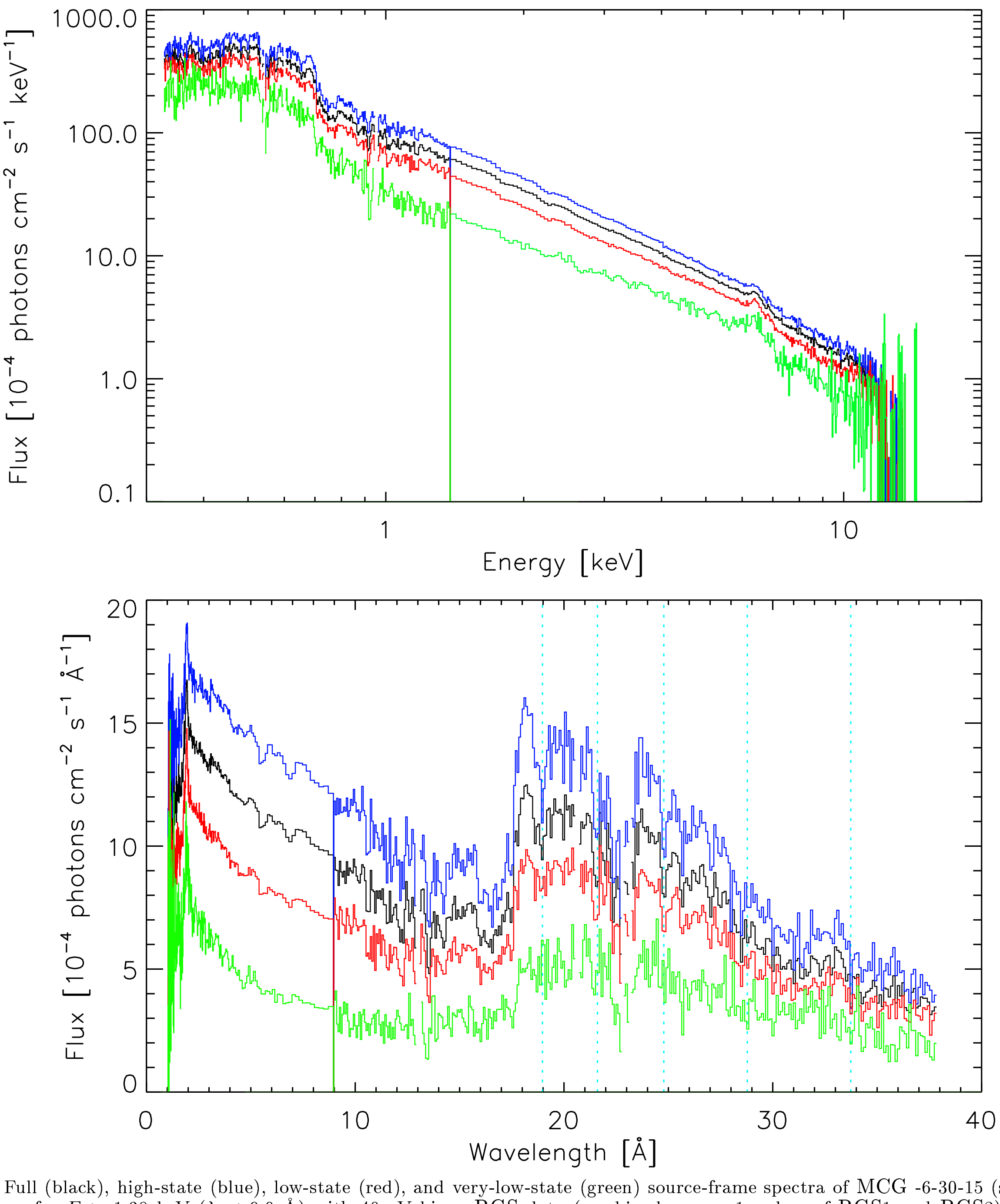

FIG. 10.— Full (black), high-state (blue), low-state (red), and very-low-state (green) source-frame spectra of MCG -6-30-15 (see Fig. 1). PN data shown for $E > 1.38$ keV ($\lambda < 9.0$ Å) with 40 eV bins. RGS data (combined $m = -1$ orders of RGS1 and RGS2) shown for $E < 1.38$ kev ($\lambda > 9.0$ Å) with roughly 40 mÅ bins. Vertical lines correspond to wavelengths of O VIII Lyα, O VII r, N VII Lyα, N VI r, and C VI Lyα

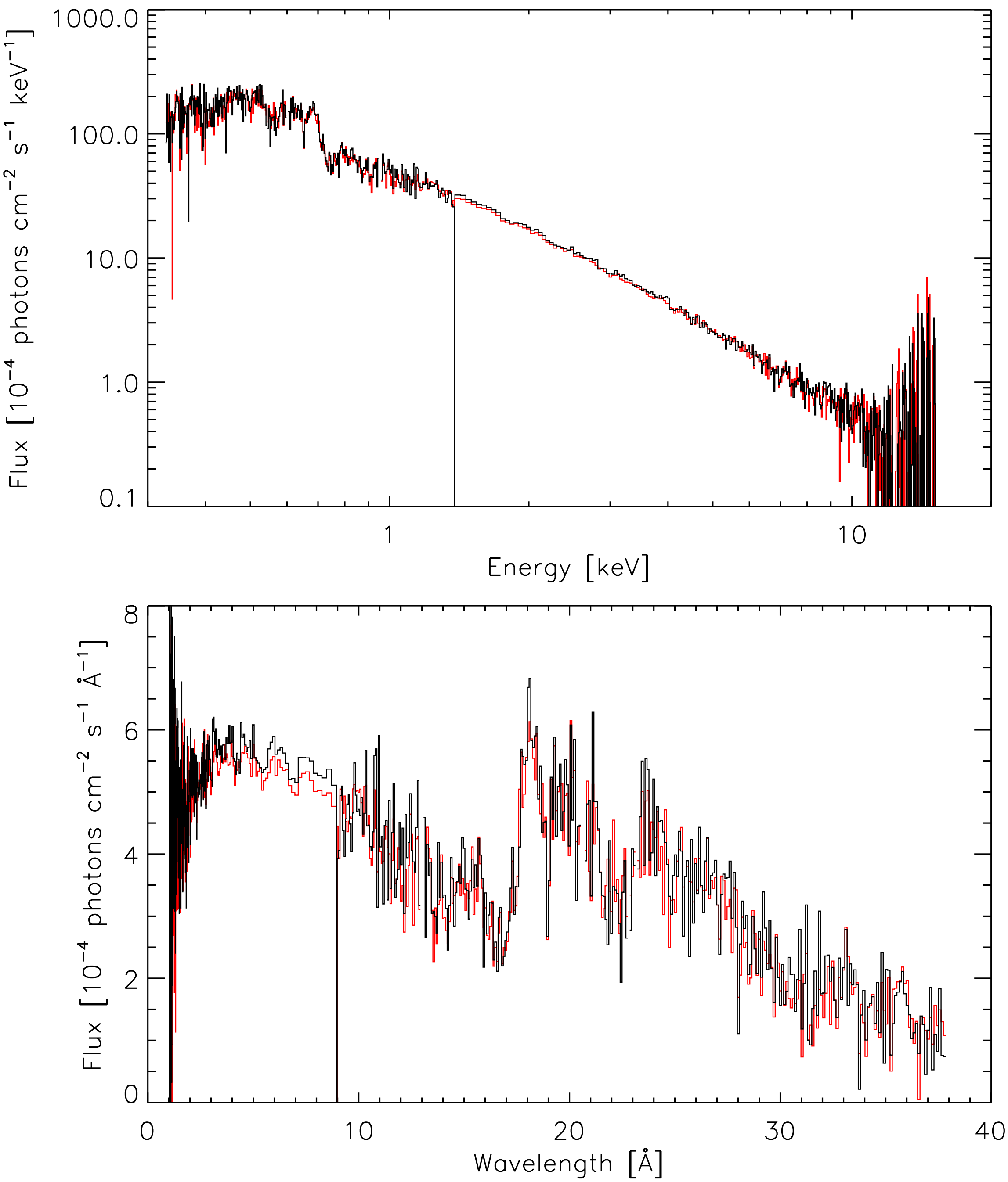

FIG. 11.— Difference spectra constructed from spectra shown in Fig. 10, corresponding to high-state minus low-state (black) and high-state minus very-low-state (red; scaled by 0.55). (Same plotting conventions as in Fig. 10.)

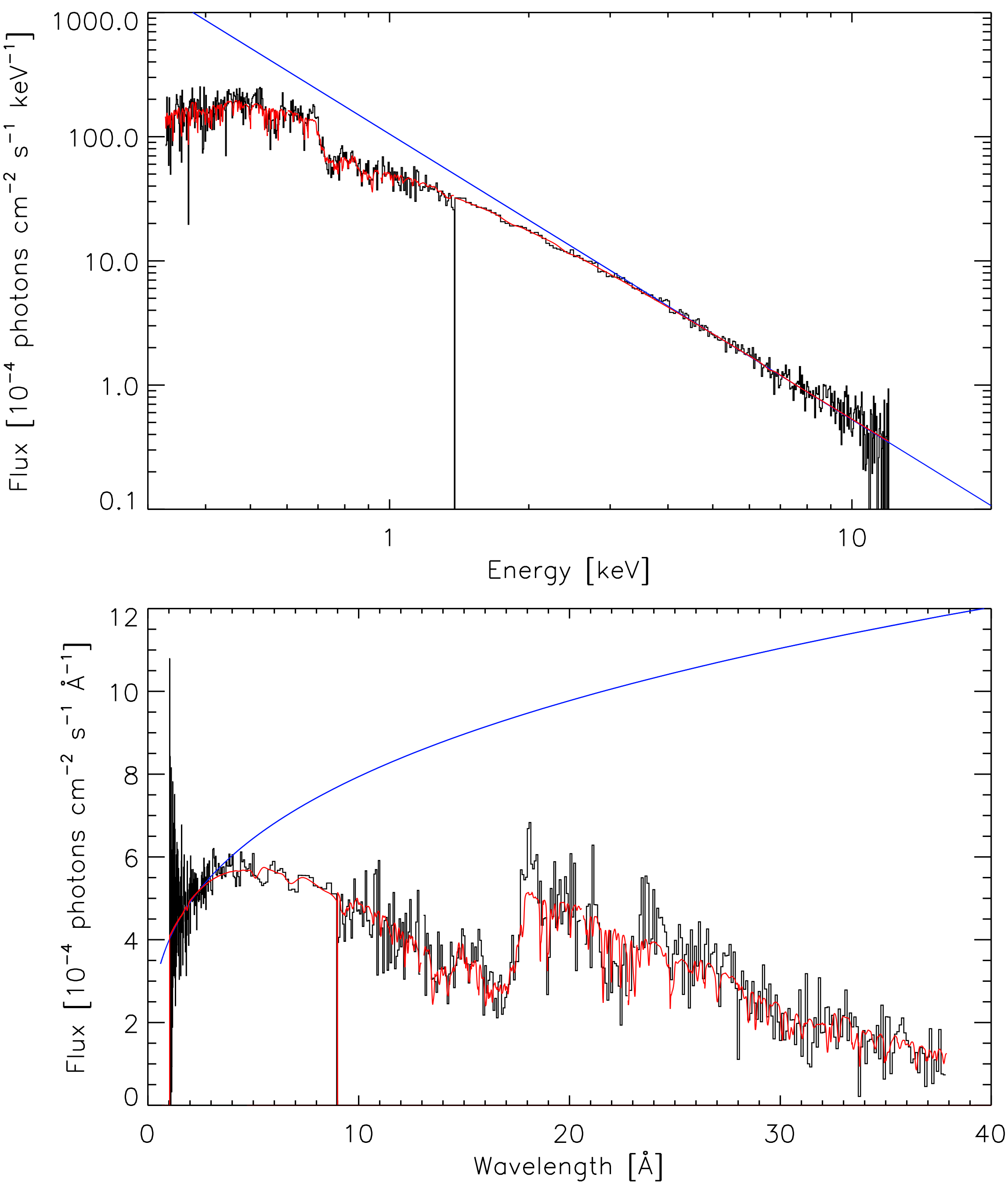

FIG. 12.— High-state minus low-state difference spectrum of Fig. 10 shown in black. The $\Gamma = 2.3$ power-law fitted to high energies is shown in blue, and the intrinsic ionic absorption (with Milky Way absorption included as well) is shown in red. No discrete absorption features are detected above ~ 4 keV. (Same plotting conventions as in Fig. 10.)

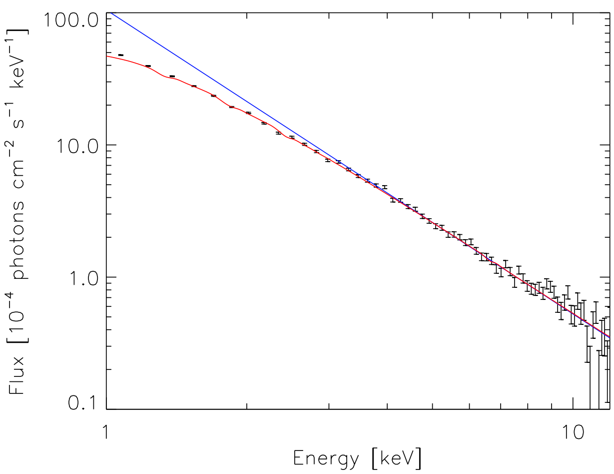

FIG. 13.— Zoomed-in view of 1–12 keV region of Fig. 12 showing the absence of features in the power law above 4 keV. Bins are 160 eV.

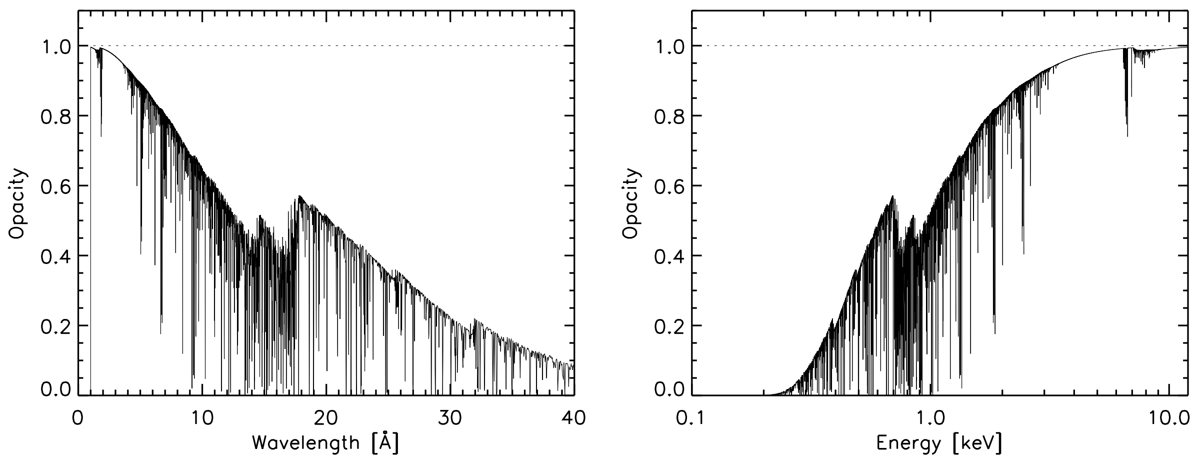

FIG. 14.— Ionic opacity used in Fig. 12 (Milky Way opacity and blueshift have been removed).

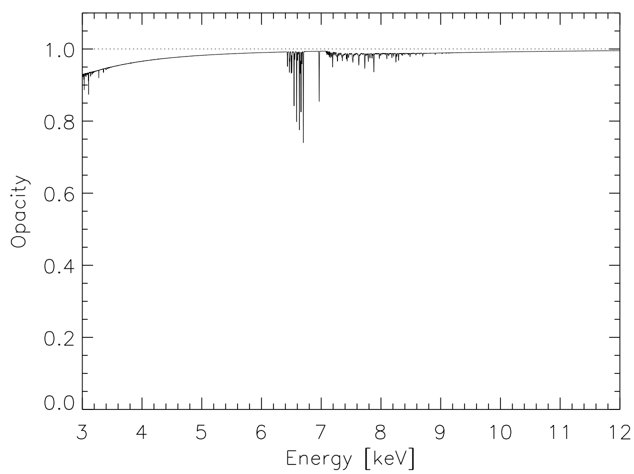

FIG. 15.— Predicted Fe K-shell opacity for MCG -6-30-15.

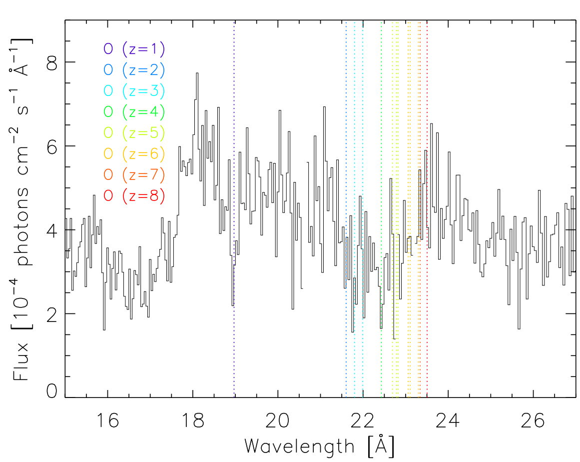

FIG. 16.— Zoomed-in view of the O K-shell region of the bottom panel of Fig. 12. All significant 1s→2p transitions from all charge states of O (from $z = 1$ to 8 electrons). Bins are roughly 20 mÅ.

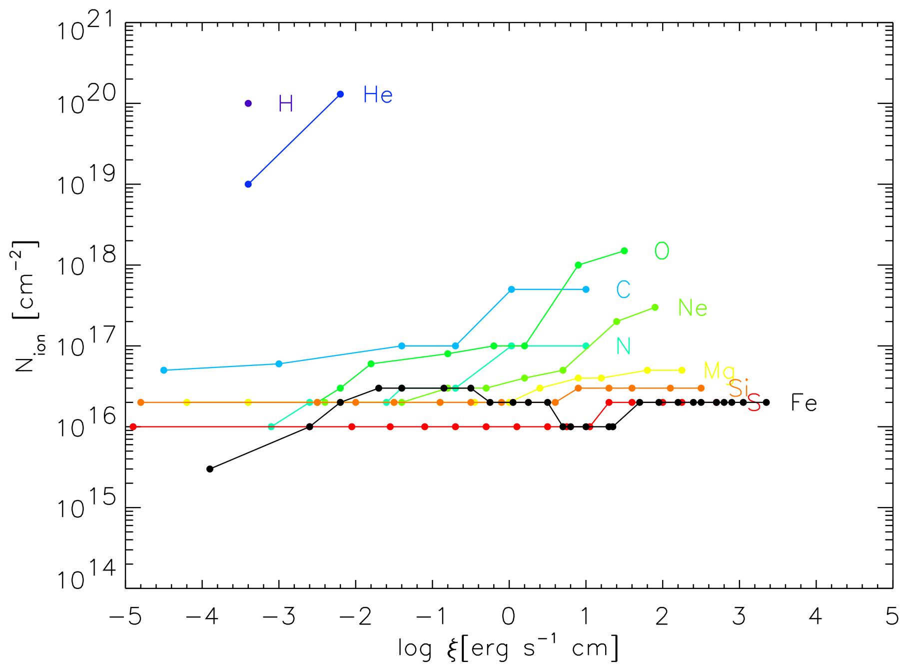

FIG. 17.— The ionic column densities used to fit the spectrum of MCG -6-30-15 shown in Fig. 12.

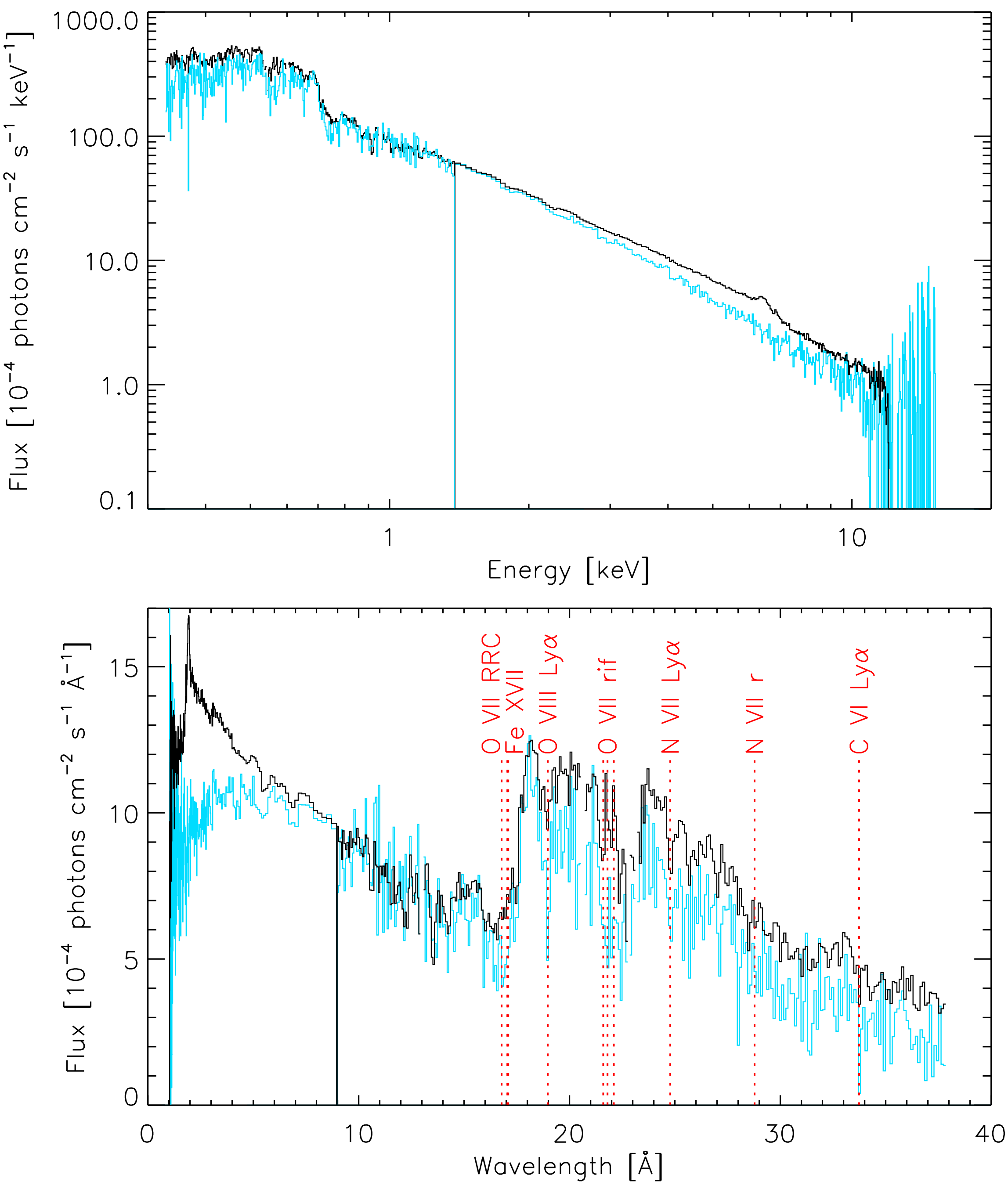

Fig. 18.— Multiplying the difference spectrum (high-state minus low-state) by 1.85 pushes it up to the total spectrum to a level where the first few bins are coincident. Any discrete features which appear here must also appear in the constant spectrum. (Same plotting conventions as in Fig. 10.)

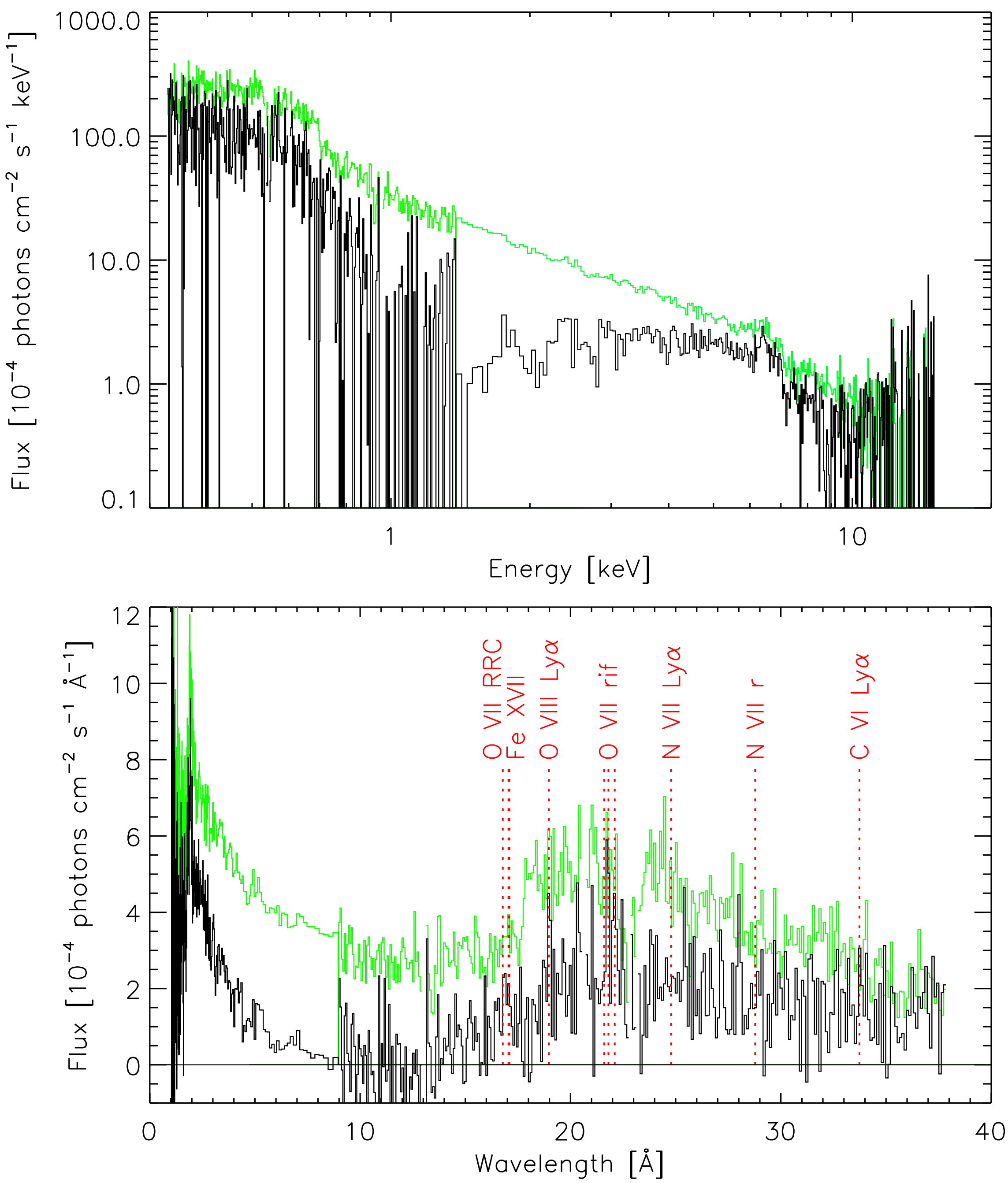

Fig. 19.— By subtracting off the difference spectrum (Figs. 11), we obtain a lower limit to the constant spectrum. An upper limit is given by the very-low-state spectrum. The true constant spectrum lies somewhere in between these two extremes. (Same plotting conventions as in Fig. 10.)

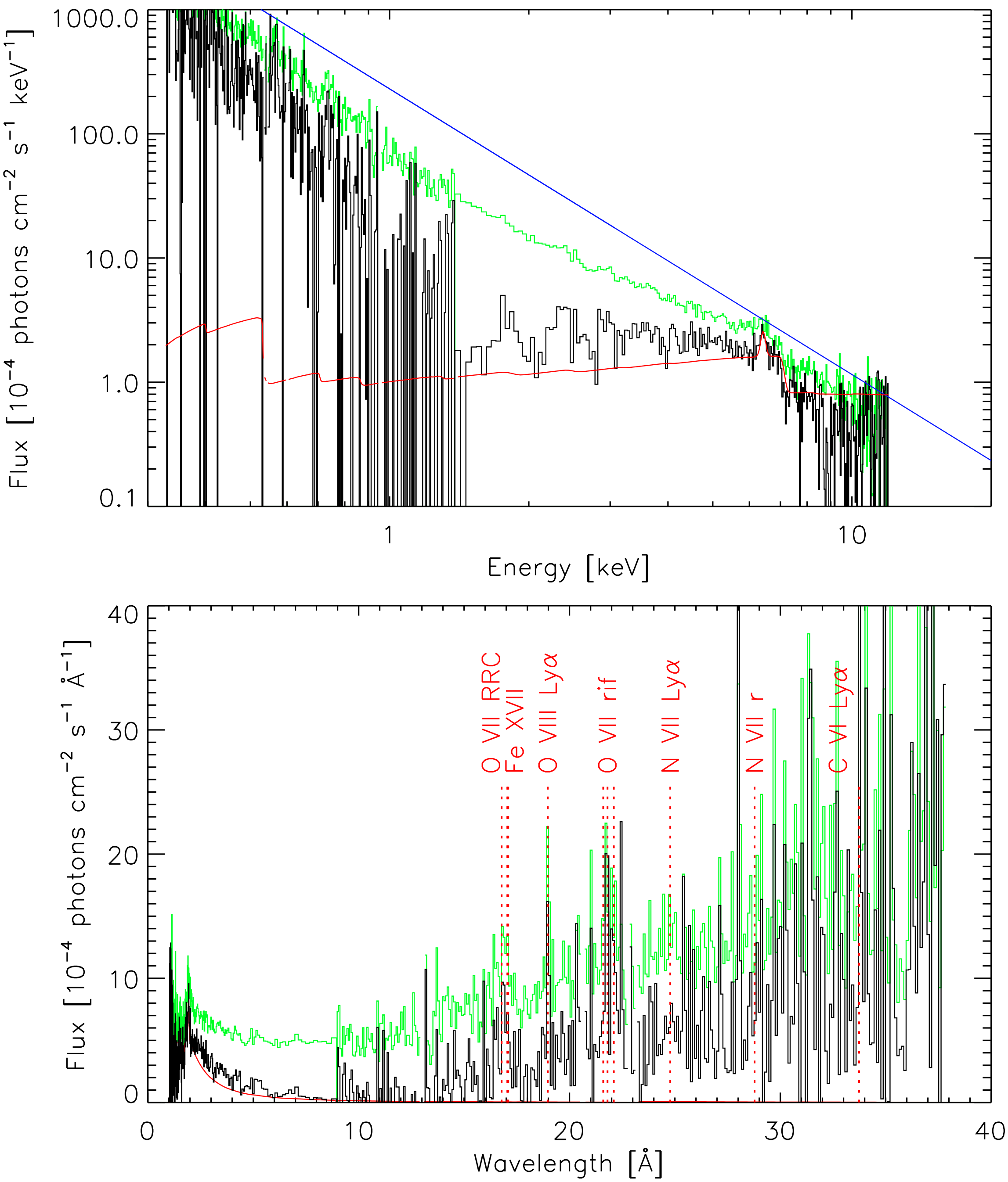

FIG. 20.— Constant spectrum lower limit (from Fig. 19) with absorption removed by dividing out the observed absorption (both ionic absorption and Milky-way absorption), assuming the same $\Gamma = 2.3$ power law as shown in Fig. 11. (Same plotting conventions as in Fig. 10.)

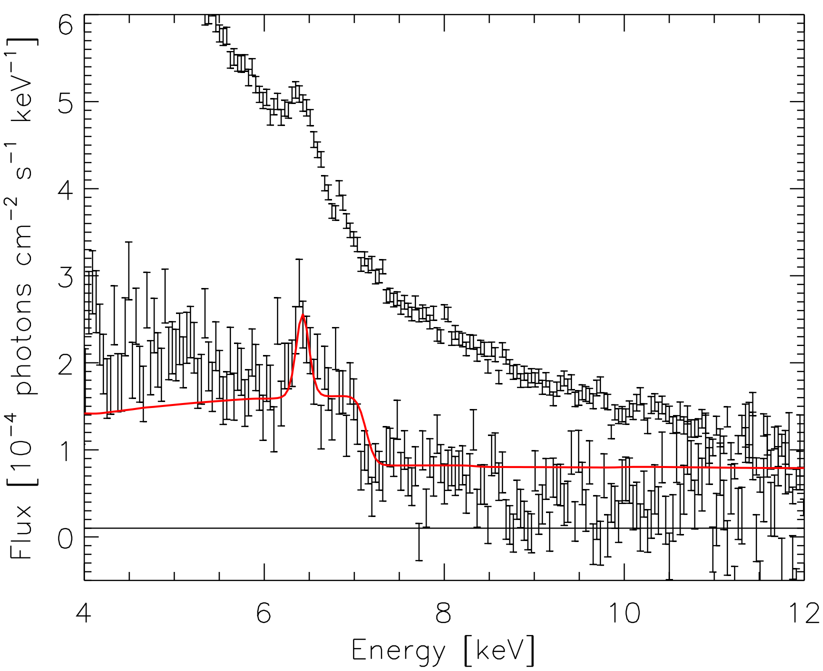

FIG. 21.— Zoomed-in view of top panel of Fig. 20 for the Fe K region. Also shown above the constant spectrum is the full PN spectrum. Bins are 40 eV.

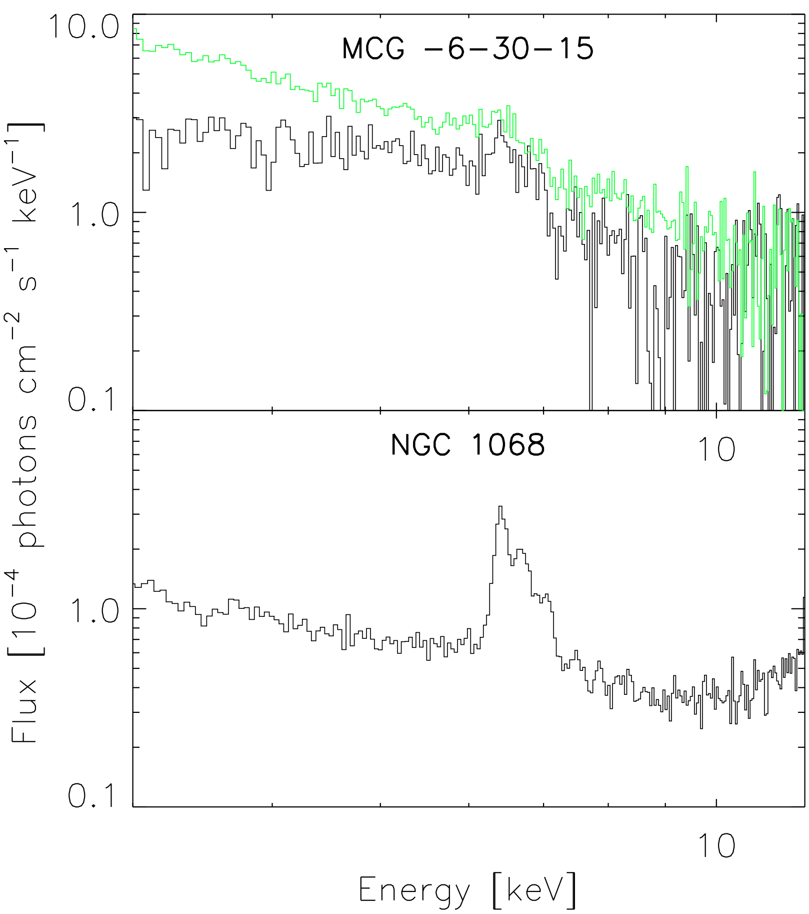

FIG. 22.— Comparison of Fe K regions for the constant component of MCG -6-30-15 and the spectrum of NGC 1068. For MCG -6-30-15, the upper and lower limits (with absorption divided out) are shown (identical to Fig. 20). Bins are 40 eV.

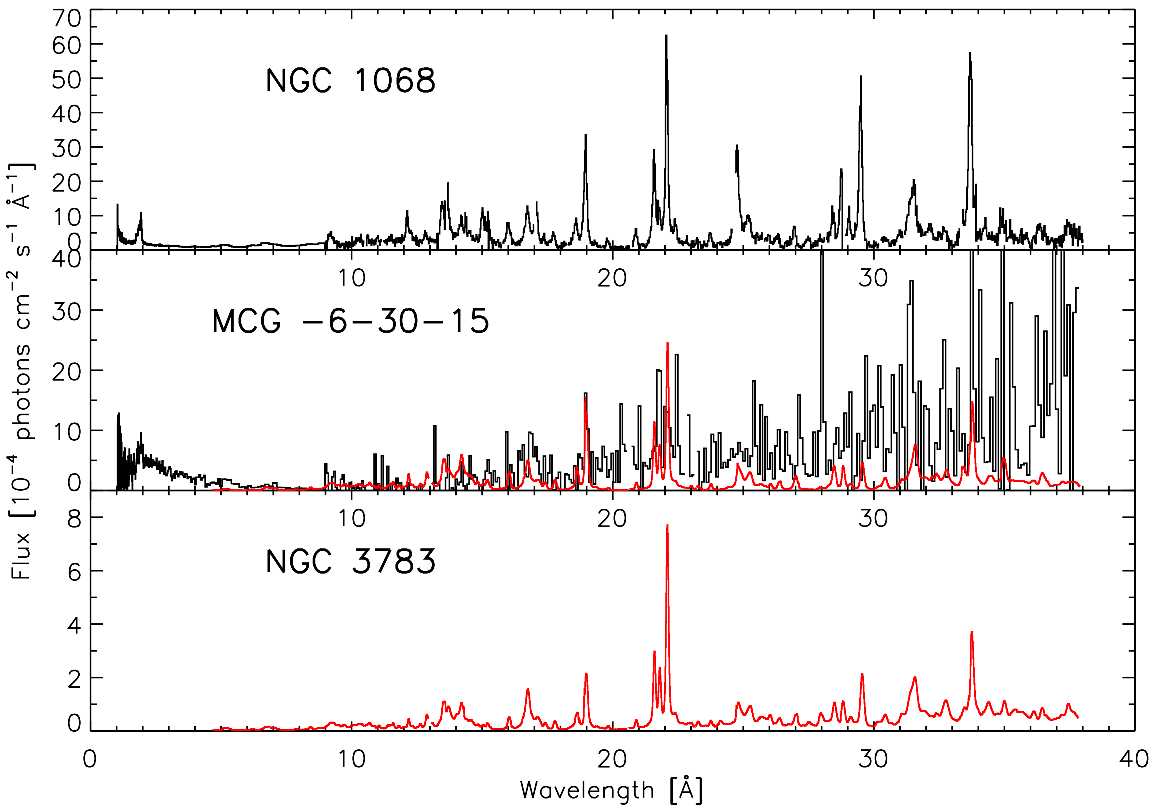

FIG. 23.— Taking the column densities assumed in Figs. 6 and 12, we plot what NGC 3783 and MCG -6-30-15 would look like as Seyfert 2 galaxies (see Kinkhabwala et al. 2003 for more details on this procedure). The RGS1 spectrum ($m = -1$ order) of the prototypical Seyfert 2 galaxy NGC 1068 (Kinkhabwala et al. 2002) is shown in the top panel, the predicted, Seyfert-2-like spectrum of MCG -6-30-15 in the middle panel (red), and the predicted, Seyfert-2-like spectrum of NGC 3783 in the bottom panel (red). For the MCG -6-30-15 panel, we also once again show the lower-limit spectrum (with absorption divided out) from Fig. 20. Binning is the same as for Fig. 10. See text for more details.